Biomedical Signal Processing and Control 76 (2022) 103725

Contents lists available at ScienceDirect

Biomedical Signal Processing and Control

journal homepage: www.elsevier.com/locate/bspc

# Multigroup recognition of dementia patients with dynamic brain connectivity under multimodal cortex parcellation

Bocheng Wang [a,*], Lei Li [a], Long Peng [a], Zhuolin Jiang [a], Kexuan Dai [a], Qi Xie [a], Yue Cao [b], Dingguo Yu [a], for the Alzheimer's Disease Neuroimaging Initiative

[a] College of Media Engineering, Communication University of Zhejiang, Hangzhou, Zhejiang 310018, China
[b] Department of Radiology, The First Hospital of Jilin University, Changchun, Jilin 130021, China

ARTICLE INFO

*Keywords:*
HCP MMP
Dynamic Connectivity
Alzheimer's Disease
Resting-State Network
Deep Learning
Graph-based Analysis

ABSTRACT

*Objective:* To accurately predict Alzheimer's disease (AD) in its early stage of cognitive impairment is crucial to clinical diagnosis and intervention. However, there is no consensus over which parts of brain areas are responsible for cognitive decline due to the incompatible and single-modal-based parcellation methods employed by researchers.

*Methods:* A novel dynamic brain connectivity processing method (DBCP) is proposed based on the human connectome project multimodal parcellation (HCP MMP) to explore the spatial–temporal characteristics of the brain in different stages of mild cognitive impairment (MCI) and Alzheimer's disease. First, dynamic connectivity under HCP MMP is constructed to divide the whole fMRI time series into hundreds of segmentations. Then, graph-based topological measures are calculated, followed by statistical outlier examinations implemented by the K-means method.

*Results:* A superior performance (accuracy = 86%, recall = 87%, precision = 86%, F1-score = 86%) in the four groups (healthy control vs. early MCI vs. late MCI vs. AD) recognition is achieved by training an effective but uncomplicated deep learning model.

*Conclusion:* Dynamic connectivity within the most fine-grained multimodal human cortex parcellation can reveal more useful details to distinguish brain dysfunctional patients compared with static connectivity or single modal based parcellation, and the proposed method can suppress the outliers well among fragmented fMRI signals.

*Significance:* Providing more evidence on the primary responsibility of DMN and DAN for cognitive impairment of the brain, 64 cortex regions with significant topological alterations are suggested as the most prominent and fine-grained biomarker for further longitudinal AD studies.

## 1. Introduction

Dementia is becoming an increasingly social problem worldwide and is one of the major causes of dysfunctionality in the human brain. Alzheimer's disease (AD), the most common form of dementia, contributes to nearly 60%-70% of cases and is accompanied by severe memory loss, decreased language expression, decreased social ability decline, and many other behavioral issues. AD is a chronic neurodegenerative disease that gradually worsens over time, so it is crucial to intervene and treat patients in the early stage of AD. Mild cognitive impairment (MCI) is considered a transitional stage between normal aging and AD. In the Alzheimer's Disease Neuroimaging Initiative (ADNI), patients are categorized by their neuropsychological examination scores, such as the Clinical Dementia Rating Scale (CDR) and Mini-Mental State Examination (MMSE), into cohorts of early MCI (EMCI), late MCI (LMCI) and AD. Studies around the world aim to achieve accurate predictions based on various methods before deteriorating to an irreversible state, and great progress has been made in recent years. Sarraf et al., [1] collected two subsets of the ADNI database with structural MRI and resting-state functional MRI (rs-fMRI) data, aligned the registered images to the MNI152 standard space, and finally achieved an accuracy of 99.9% in the classification of AD and healthy controls (HCs). Hu et al., [2] investigated 549 subjects from the ADNI database and preprocessed the MRI data with a standard voxel-based morphometry method, extracted multiscale features for both whole gray matter images and gray matter images of the hippocampus region, and recognized AD patients from HC

* Corresponding author.
*E-mail address:* wangboc@cuz.edu.cn (B. Wang).

https://doi.org/10.1016/j.bspc.2022.103725
Received 22 January 2022; Received in revised form 19 March 2022; Accepted 9 April 2022
Available online 15 April 2022

with an accuracy of 84.13%. Hojjati et al., [3] acquired 18 patients who converted to AD from MCI (cMCI) and 62 age-matched MCI non-converters with structural and functional MRI images, tested the statistical significance of computed features, and trained a classification model with an accuracy of 91.4%. Although the performance of binary-group classification is excellent, an important remaining problem is that most trained models are incompetent to obtain high accuracy in multi-group distinguishment among HC, EMCI, LMCI, or AD, mainly because the patterns in brain characteristics related to human cognitive impairment has not yet been properly grasped.

An increasing number of studies [4–6] confirm that cognitive impairment is induced by regional dysfunction in the brain instead of the whole. A common preprocessing used to study the brain's regional functionality is parcellation. There are kinds of methods for brain segmentation in terms of structure or function employed by studies for dementia. Hojjati et al., [7] adopted the Automated Anatomical Labeling (AAL) atlas to extract 90 regions of interest (ROIs), calculated functional connectivity matrices for 80 MCI patients, and finally selected the optimal six features for the classification with high accuracies. Suk, H. I et al., [8] parcellated the brain into 93 ROIs by warping the Kabani atlas and trained a deep learning model for the diagnosis of AD/MCI. Grajski and Bressler [9] segmented the brain into cortical parcellation and subcortical regions by using FreeSurfer and Analysis of Functional NeuroImages (AFNI) software and proved that resting-state functional connectivity in the medial temporal lobe (MTL) can be a candidate biomarker of Alzheimer's neuropathology. Most of the parcellation atlases in these studies were constructed by a single modality, and it is inconsistent and not compatible with the naming and sizing of parcellated areas. Generally, for comparison, these studies must map brain regions into the Brodmann areas which were proposed back in 1909. In 2016, a novel parcellation method (HCP MMP, human connectome project multimodal parcellation) [10] based on sharp changes in cerebral cortical architecture, function, connectivity, and topography, was delineated with 180 areas per hemisphere. It is considered the most fine-grained to date human parcellation method and is expected to study the brain functioning mechanism at a multimodal level. Although HCP MMP charactered the details for a healthy brain, there is a lack of research on aging or diseased brains, particularly those that focus on AD patients. In addition, it is largely limited by the high quality of T1/T2w images required and sophisticated preprocessing to carry out. Recently, a more general solution to this problem was developed by Sheng et al., [11,12] that a variety of neuroscience technologies were integrated for the registration from non-HCP ADNI data to the Connectivity Informatics Technology Initiative (CIFTI) gray-ordinate space. Previously, we compared the classification capability between HCP MMP with other atlases in static connectivity, which showed superior performance in binary recognition for AD patients with healthy controls [12,13]. However, the brain functions time-varying. The above methods did not investigate the dynamic characteristics for AD brains, and only static connectivity under HCP MMP was studied. Static correlations between fMRI BOLD signals may fail to reveal the intrinsic dynamic characteristics.

For the research of brain functionality with fMRI data, a connectivity matrix is widely constructed by computing the Pearson coefficient of the BOLD signal time series associated with voxels or regions. Other connectivity estimation measures, such as precision matrices or partial correlations, have also been mentioned in the literature [14]. Usually, the connectivity of any two areas is calculated by using the whole range of time series, and it is considered an average level of associations between regions in the brain and referred to as static connectivity. The advantages of this approach are that noise generated during fMRI scanning can be weakened and that the method is easy to implement without many parameters to set. Recently, the time-varying connectivity network chronnectome [15] has attracted great interest [16–18], which focuses on the spatiotemporal dynamic characteristics of brain functionality. A sliding window is employed to divide the fMRI time series into several consequent segmentations in which the functional connectivity networks are calculated separately. Moguilner et al., [19] calculated both static and dynamic connectivity from 300 participants' resting-state fMRI data, and an accuracy of 86.63% was yielded in the AD vs. HCs binary classification. While, windowed time series also induce lots of meaningless fMRI fragments which come from an intact signal sequence, which leads to numerous outliers in significance statistics. There is no conclusion as to whether this method helps improve accurate prediction in multigroup situations and precisely locating the regions of pathological changes in the brain.

In this study, we propose a novel method (DBCP) based on HCP MMP to explore the dynamic characteristics of the brain in different stages of MCI and AD patients and designed an efficient deep learning model with high accuracies in four-group (HC vs. EMCI vs. LMCI vs. AD) recognition. To the best of our knowledge, it is the first time to integrate multimodal cortex parcellation with chronnectome for AD study. The DBCP steps are described in the Materials and Method section. Various aspects of static and dynamic connectivity networks in statistics and classification are compared in the Results and Discussion section. Significantly altered HCP MMP areas are mapped into widely accepted intrinsic resting-state networks (RSNs) [20]. Results show that dynamic connectivity within the most fine-grained multimodal human cortex parcellation can reveal more useful details to distinguish brain dysfunctional patients compared with static connectivity or single modal based parcellation, and the outliers among fragmented fMRI signals can be well suppressed by DBCP. It provides more evidence on the primary responsibility of the default mode network (DMN) and dorsal attention network (DAN) for cognitive impairment of the brain.

## 2. Materials and method

Fig. 1 shows the DBCP workstream proposed in this study.

### 2.1. Data acquisition

A total of 160 subjects from the ADNI2 dataset were acquired with structural and functional MRI data in this study. To ensure the consistency of the imaging protocol across the four cohorts and the robustness of the results, for the structural MRI data, subjects scanned only by Philips Medical Systems with T1 weighting (Magnetization Prepared Rapid Gradient Echo, MPRAGE) were collected. The spatial resolution = 256 × 256 × 170 pixels, the pulse sequence is GR, the slice thickness = 1.2 mm, TE = 3.1 ms, and TR = 6.8 ms. For the functional MRI data, subjects in the resting state with eyes open were gathered. The spatial resolution = 64 × 64 × 48 pixels, the pulse sequence is GR, the slice thickness = 3.3 mm, TE = 30 ms, and TR = 3000 ms. The number of slices is 6720. The total number of fMRI volumes is 6720/48 = 140. Subjects were classified into EMCI, LMCI, AD, and HC according to their baseline/screening visit neuropsychological assessments. Table 1 shows the demographic information and neuropsychological assessments of subjects employed in this study and more details are listed in Supplementary Table 1.

### 2.2. Dynamic brain connectivity in HCP MMP

The whole brain of each subject was first parcellated into 360 cortical areas by the definition of HCP MMP using JHCP MMP [11]. First, structural and functional MRI data acquired from ADNI were registered into the standard CIFTI gray-ordinate space [21], which contains 26,298 subcortical voxels in 2 mm Montreal Neurological Institute (MNI) space and 32,492 surface vertices per hemisphere. Next, the template of HCP MMP was adapted to parcellate these 32,492 vertices per hemisphere into 180 cortical areas per hemisphere. For comparison, the commonly accepted functional networks of the human brain, resting-state networks (RSNs) or intrinsic connectivity networks (ICNs), were adopted to map the 360 cortical adjacent regions into seven

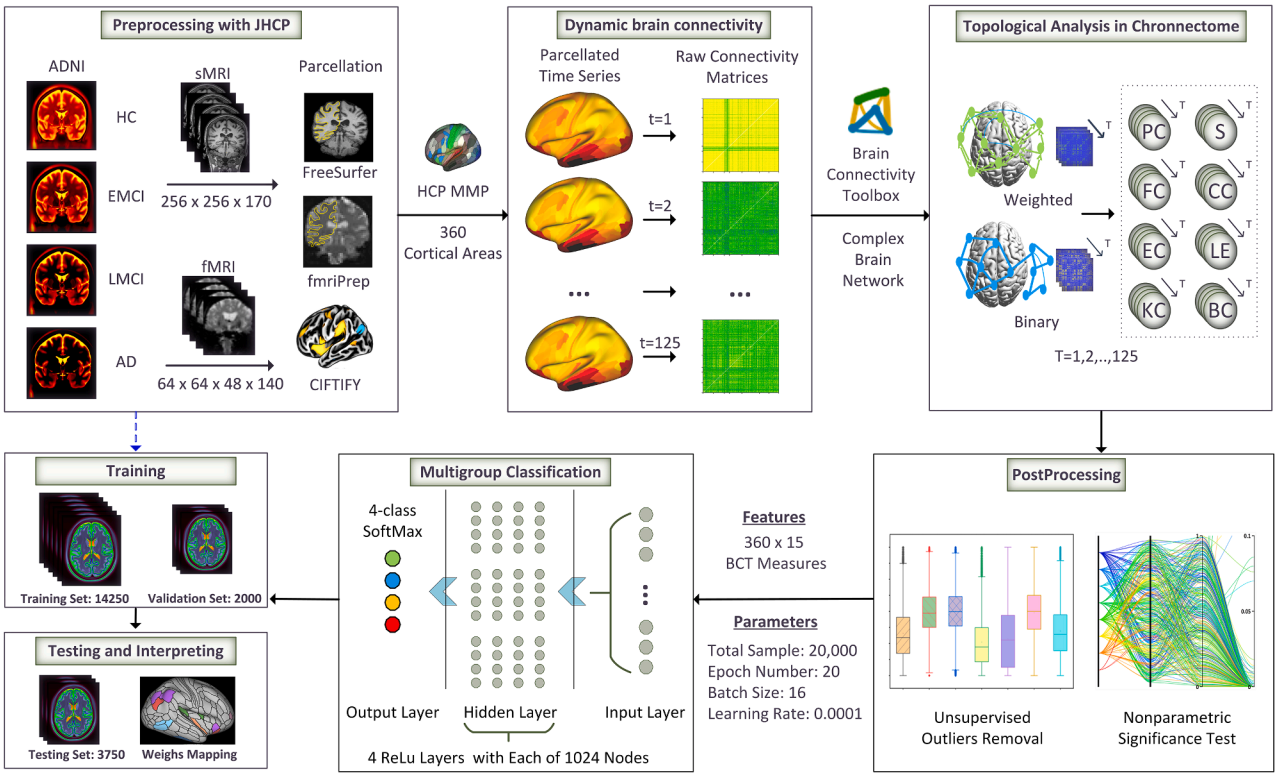


**Fig. 1.** The DBCP workstream proposed in this study.

**Table 1**
Demographic information and neuropsychological data.

| | HC | EMCI | LMCI | AD |
|---|---|---|---|---|
| Total number | 43 | 53 | 34 | 30 |
| Male/Female | 16/27 | 20/33 | 21/13 | 12/18 |
| Age | 75.51 ± 6.27 | 71.68 ± 6.39 | 72.35 ± 8.26 | 73.10 ± 6.81 |
| MMSE | 28.93 ± 1.25 | 28.21 ± 1.72 | 27.79 ± 1.66 | 22.73 ± 2.45 |
| CDR | 0.00 ± 0.00 | 0.49 ± 0.07 | 0.50 ± 0.00 | 0.85 ± 0.23 |
| NPI | 0.73 ± 1.13 | 3.35 ± 5.58 | 3.37 ± 4.05 | 9.93 ± 10.68 |
| GDS | 0.70 ± 1.07 | 1.89 ± 1.54 | 1.59 ± 1.42 | 1.50 ± 1.06 |
| FAQ | 0.11 ± 0.38 | 2.49 ± 3.92 | 3.97 ± 4.48 | 15.62 ± 7.23 |
| ADAS | 9.00 ± 3.50 | 12.64 ± 5.23 | 17.10 ± 7.25 | 35.54 ± 8.58 |
| ADNI_MEM | 1.00 ± 0.51 | 0.55 ± 0.57 | 0.10 ± 0.54 | −1.04 ± 0.54 |
| ADNI_EF | 0.83 ± 0.70 | 0.57 ± 0.79 | 0.18 ± 0.99 | −1.11 ± 0.72 |

MMSE: Mini-Mental State Examination. CDR: Cognitive Dementia Rating Scale. NPI: Neuropsychiatric Inventory. GDS: Geriatric Depression Scale. FAQ: Functional Activities Questionnaire. ADAS: Alzheimer's Disease Assessment Scale. ADNI_MEM and ADNI_EF: Composite measures of executive function and memory derived by ADNI.

physically disconnected functional networks consisting of the default mode network (DMN), dorsal attention network (DAN), somatomotor network (SN), frontoparietal network (FN), visual network (VN), ventral attention network (VAN) and limbic system.

In both static and dynamic connectivity, the graph theory-based method was adopted by which parcellated regions are considered nodes in the graph. The correlation coefficient of the regional fMRI time series was computed as the weighting edge and forms the connectivity between brain regions. In general, static brain connectivity was measured for the average BOLD signal of the overall fMRI time series data from a single subject, and dynamic connectivity focused on investigating the time-varying characteristics of the brain. In this study, the spatiotemporal resolution of fMRI data was 64 × 64 × 48 (pixels) × 140 (volumes). We set up a fixed sliding window for segmentations of the overall fMRI time series. The size of the sliding window was 15, and the sliding step was 1. This means that there were 125 windowed time series segmented from the original fMRI time series, and each window involved 15 volumes and moves forward one volume each time for the next windowed time series. In HCP project, the parcellated fMRI data was stored in a *.ptseries file. Thus, the whole time series in the *.ptseries file was segmented by these 125 windows. The correlation coefficients were calculated among 360 areas in paired windowed signals to construct the connectivity matrix. Consecutive connectivity matrices formed the chronnectome in the brain. In this way, the size of limited subjects was enlarged from 160 to 20,000 (160 × 125), which greatly increased the amount of available data.

### 2.3. Topological alterations in the chronnectome

Centrality change in brain connectivity is considered an important characterization in Alzheimer's disease and has been widely studied in literatures. Brain function is an interactivity result of brain regions. Study on the communication structure or information transmission path is expected to explain the functional mechanism of brain. In network-based analysis, brain areas are defined as the nodes. Centrality quantifies the importance of these nodes in communication. Based on the dynamic brain connectivity networks that originate from the fMRI time series, centralities in complex brain networks were computed. The regional characteristics of each node in the connectivity were analyzed. Strength (S), clustering coefficient (CC), local efficiency (LE), betweenness centrality (BC), page rank centrality (PC), eigenvector (EC), flow coefficient (FC), and k-coreness centrality (KC) were computed. All these measures have been defined previously in the literature to characterize topological alterations in brain function and have been implemented in various software packages. In this study, these are referred to as BCT measures because they are calculated within the brain connectivity toolbox (BCT) [22].

### 2.4. Statistical outlier removal by unsupervised learning

Before the subsequent analysis and deep learning, BCT measures

should be tested to verify the statistical significance and effectiveness for classification in cohorts of different stages of MCI and AD patients. Although the processes of thresholding and binarization are carried out to achieve data enhancement, there still exists much noise and redundant information in the data for training. However, the commonly used parametric significance tests cannot be directly used here due to the unknown distributions of the BCT measures in brain networks. Two steps were implemented to improve data quality. First, a nonparametric significance test followed by FDR correction was adopted to test the significance of BCT measures in both static and dynamic functional brain connectivity. According to the Kruskal-Wallis H theory, a significance value beyond 0.05 implies an invalid statistical test that may be an accidental result. Only features with significant differences below 0.05 level among groups were retained. Second, the unsupervised machine learning K-means method was used for the removal of outliers, especially for dynamic connectivity, as the postprocessing procedure follows a significance test. Initially, K was set to 2, corresponding to the normal observations and outliers. The sigma principle derived from the normal distribution was considered as the convergence thresholding during iterations in K-means. By calculating the distance between these values, noise information can be clustered and removed. Combined with boxplot, outliers in BCTs can be removed observably. Outliers are not the dynamic connectivity itself, but the calculated BCT measures based on that. Finally, only valid BCT measures were passed to the deep learning model in Section 2.5.

### 2.5. Multigroup classification with dynamic characteristics

To compare the effectiveness of BCT measures in static and dynamic connectivity for recognition in four-group subjects, a deep learning model was designed with fewer customized parameters than other complex models. In the input layer, 360 regional values from one of the fifteen BCT measures, which were computed from either static or dynamic connectivity and processed by statistical outlier removal, were normalized to [0, 1] to feed the training model.

The hidden layer consisted of four sublayers, and in each of the sublayers, there are 1024 rectified linear unit (ReLU) activation nodes. In the output layer, we adopted a four-class softmax structure for the determination of the testing subject belongs. The initial learning rate was 0.0001. The number of training iterations (epochs) was set to 20, and the batch size of the training samples was set to 16. These are convention settings in deep learning. Data samples are always divided into training and testing parts in a ratio of 0.8:0.2. For the avoidance of model overfitting, a validation part can be introduced, resulting in a rough ratio of 0.7:0.1:0.2. In this study, samples were divided into the three parts (training, validation, and testing), and the numbers of those parts were 114, 16, 30, adding up to 160 subjects for the static analysis, and each part is further segmented into 125 windows ($114 \times 125 = 14250$, $16 \times 125 = 2000$, $30 \times 125 = 3750$, adding up to 20,000 samples) for the dynamic connectivity analysis. BCTs in different windowed connectivities that were calculated from the same subject were assigned to the same set to avoid overfitting.

## 3. Results

Fig. 2 shows the results of dynamic brain connectivity by carrying out overlapping sliding-window segmentations on the BOLD signal of fMRI time series from a single subject. The horizontal axis represents the index of 125 segmented windows, and the vertical axis is the average connectivity level computed within each windowed time series. Fluctuation is observed to cross the sliding windows. The strongest connectivity can be seen in Window = 1. This may be due to the inadaptability of the patient just after entering the MRI equipment. As the scanning process continues, this discomfort significantly decreases, accompanied by average connectivity weakening.

Following the generation of static or dynamic connectivity, local BCT measures are computed. Kruskal–Wallis H analysis was used to test the statistical significance of static and dynamic brain connectivity, and the results are drawn in Fig. 3. It comprises two parts: left, a mapping from 7-RSNs to HCP MMP; Right, significance *p-values* of BCTs in static and dynamic connectivity. In the static connectivity, local BCT measures show little significance, with most of the p-values not reaching the 0.05 level. In dynamic connectivity, BCT measures of nearly all areas of the brain achieved significant p-values far below 0.05.

Next, distributions of local BCT measures are analyzed for dynamic connectivity, and the results are drawn in Fig. 4**A**. Although local BCT measures in dynamic connectivity are statistically significant, most of the values do not exhibit normal distributions, especially those of BC. With the help of boxplots in Fig. 4**B**, it is more evident that many outliers appear above the Q3 + 1.5IQR level or lower than the Q1 – 1.5IQR level. These outliers are removed in the K-means algorithm with iterations. The results are shown in Fig. 4**C** and Fig. 4**D**, from which an

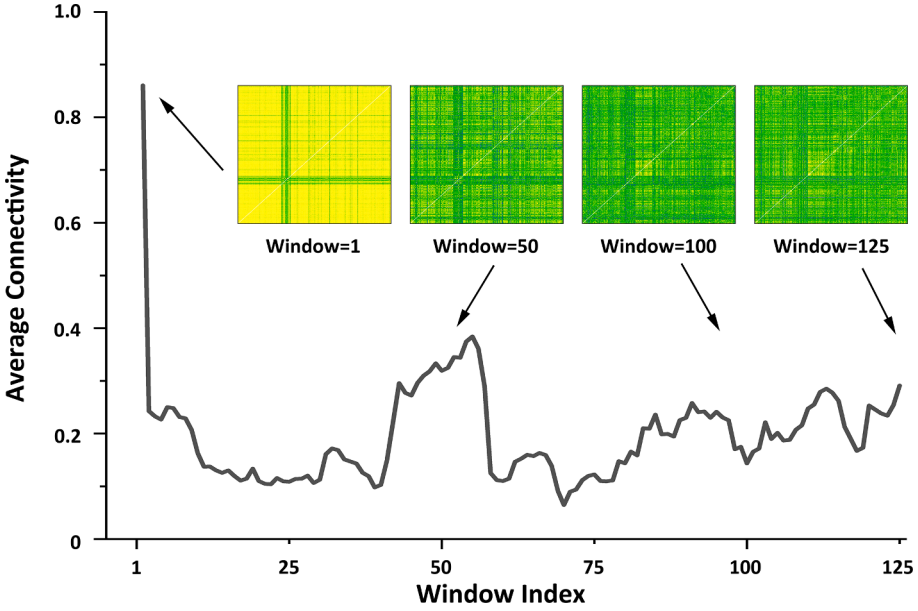


**Fig. 2.** Dynamic brain connectivity computed by 125 successive sliding windows.

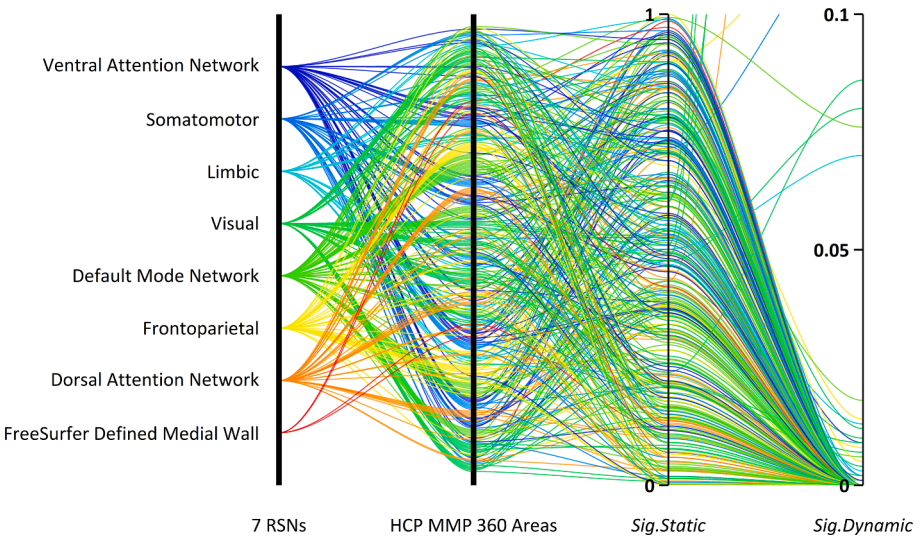


**Fig. 3.** Significance for static and dynamic functional brain connectivity. Left: The seven-RSN network areas are mapped into the HCP MMP. Right: P-value from the significance test.

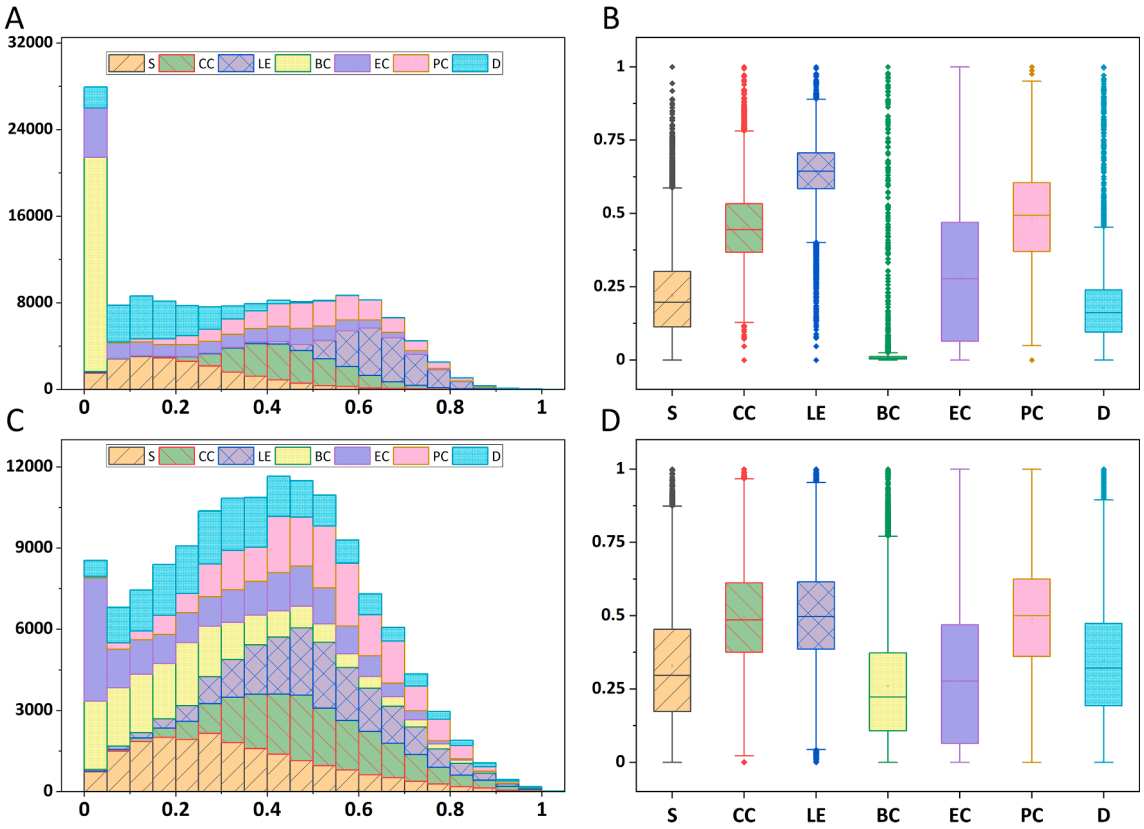


**Fig. 4.** Histogram and boxplot for the local BCT measures in dynamic brain connectivity with (A)-(B) no processing and (C)-(D) under statistical outlier removal by unsupervised learning. Data in each BCT measure are normalized to the range of [0–1] in the boxplots. Abbr. S: Strength; CC: Clustering Coefficient; LE: Local Efficient; BC: Betweenness Centrality; EC: Eigenvector Centrality; PC: Page rank Centrality; D: Degree.

approximately normal distribution can be observed and fewer outliers appear around the boxes. It can be observed that a drastic change of BC measure. This is mainly due to its complex calculation method compared to other centrality measures [22], which brings a large variation range of values.

Fig. 5 shows the classification results of different regional BCT measures in static brain connectivity, and only those of weighted networks are drawn. The horizontal axis represents the training steps, and the vertical axis represents the classification accuracy. The results in blue represent the accuracy within each training batch, and the red results are testing results during epochs in deep learning. It can be observed that most training curves continuously increase as the number of steps increases except for those in BC. Although all the final training accuracies reach approximately 100%, none of the tested models behave well in multigroup recognition, which fluctuates from 20% to 40%.

Fig. 6 shows the classification results of different regional BCT

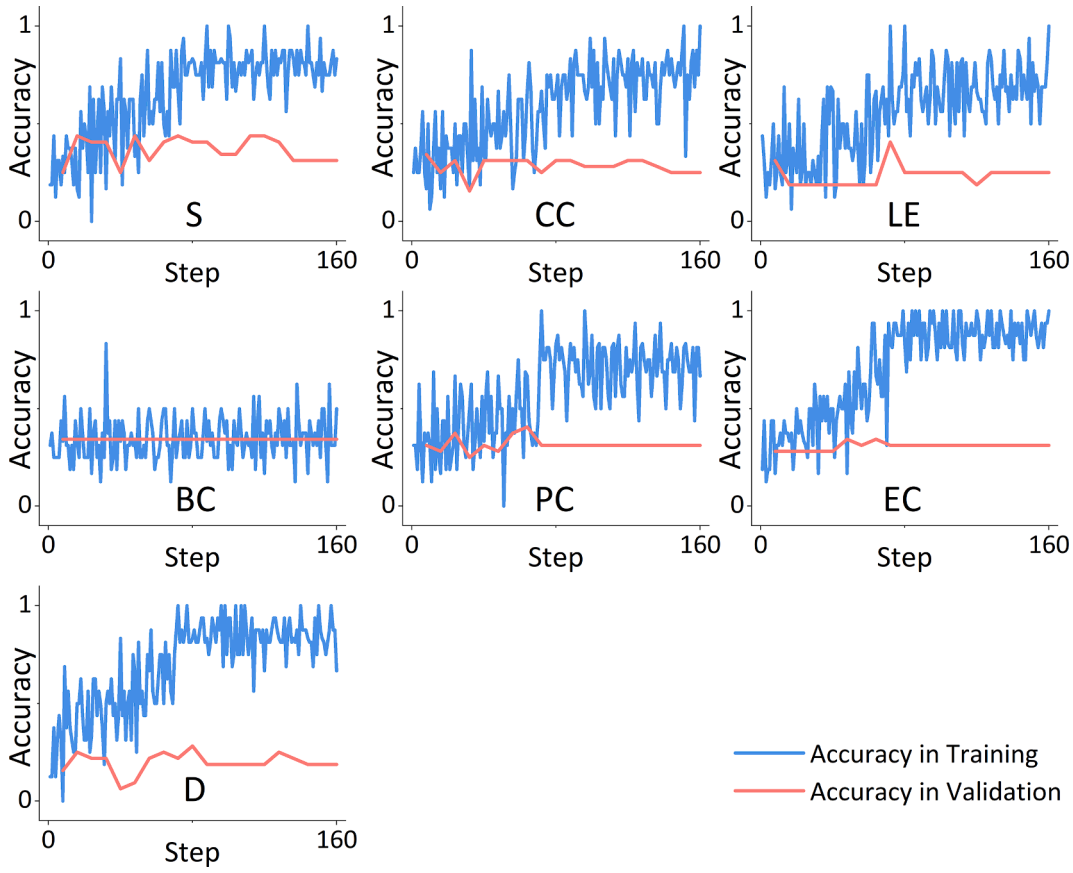


**Fig. 5.** Classification results of regional BCT measures in weighted static brain connectivity.

measures in dynamic brain connectivity without outliers' removal, and only those of weighted networks are drawn. Different from the previous Fig. 5, the number of steps (horizontal axis) increases dramatically due to its many more training samples. Despite the statistical significance drawn in Fig. 3, models trained in dynamic connectivity have not learned any effective knowledge for the four-group classification, which makes neither the training nor testing results exceed 50% accuracy, and no distinct fluctuation is observed during training. Spurious connections may be introduced during the connectivity generation [23], outliers in BCT measures dampened the performance in multigroup classification.

The curves in Fig. 7 are the training and testing results of different regional BCT measures in binary dynamic brain connectivity with outliers removed. The classification models perform better compared with the results in Fig. 5 and Fig. 6, especially the model trained on page rank topological measures. Fig. 8 and Fig. 9 illustrate the mean accuracy with error bar and confusion matrix in ten times repeated. Table 2 lists the test results of each BCT measure.

## 4. Discussion

In this study, we propose a novel fMRI data preprocessing method for the multigroup classification of different stages of MCI and AD patients. Dynamic connectivity generated in sliding windowed fMRI time series was constructed by a series of processes, including multimodal parcellation, significance testing and outlier recognition in K-means. Regional brain BCT measures were calculated for the evaluation of functional topological alterations among the four cohorts. Finally, superior performance in four-class recognition was achieved through this DBCP method, and significant changes in the cerebral cortex among different degrees of cognitive impairment were observed.

### *4.1. Significant alterations in the DMN and DAN among different stages of dementia*

We investigated the significant functional topological alterations in the brains of HCs converting to AD, and areas mapped into the seven RSNs are illustrated in Fig. 10. Following the multigroup classification, page rank is found to be the most effective feature in the recognition of different degrees of cognitive impairment. Thus, we further carried out ANOVA with Tukey's post hoc test ($p < 0.05$) on the page rank values in HCP MMP areas for all four groups of subjects. We separate the results into three parts: (A) As shown in Fig. 10**A**, alterations in these areas were significant in the HC and EMCI groups, while it failed to distinguish LMCI from AD. We consider it the early stage of HC converting to AD. These are 14 cortical areas in the DMN (R-9p, R-STSdp, L-STGa, and L-TE1m), VAN (R-p32pr, R-TPOJ1, L-FOP5), SN (R-A4, L-6mp), VN (R-V3A, L-PHA1), DAN (L-AIP), FN (L-7Pm), and limbic system (L-OFC). (B) As shown in Fig. 10**B**, the middle stage of HC converting to AD with significant differences was found in the HC and AD groups, while page rank values in these areas were not significant between the EMCI and LMCI groups. The region contains 25 areas, including DAN (R-FEF, R-7AL, R-PFt, R-FST, L-PEF, L-LIPV), DMN (R-STGa, L-PCV, L-a24, L-45, L-STSdp), VN (R-Pres, R-LO3, L-MT, L-Pres, L-PHA3, L-PHA2), FN (R-8Av, L-8c, L-i6-8), SN (L-OP4, L-A5, L-MBelt) and VAN (R-5mv, L-PI). (C) As shown in Fig. 10**C**, the last final stage of HC converting to AD with significant differences was found in the LMCI and AD groups, while page rank values in these areas were not significant between the HC and EMCI groups. The region contains 25 areas, including the DMN (R-7 m, R-POS1, R-8Ad, L-10r, L-10d, L-s6-8, L-s32), DAN (R-7Am, R-LIPv, R-IFJp, R-IPOJ3, L-7Pl), VAN (R-23c, R-p24pr, R-MI), SN (R-3a, R-A5, R-MBelt), FN (R-44, R-IFJa, L-a32pr), VN (R-MST, R-VMV2, L-V8) and limbic system (R-EC). Table 3-5 list all the details referred in Fig. 10. It is generally believed that dysfunctionality in DMN and DAN causes

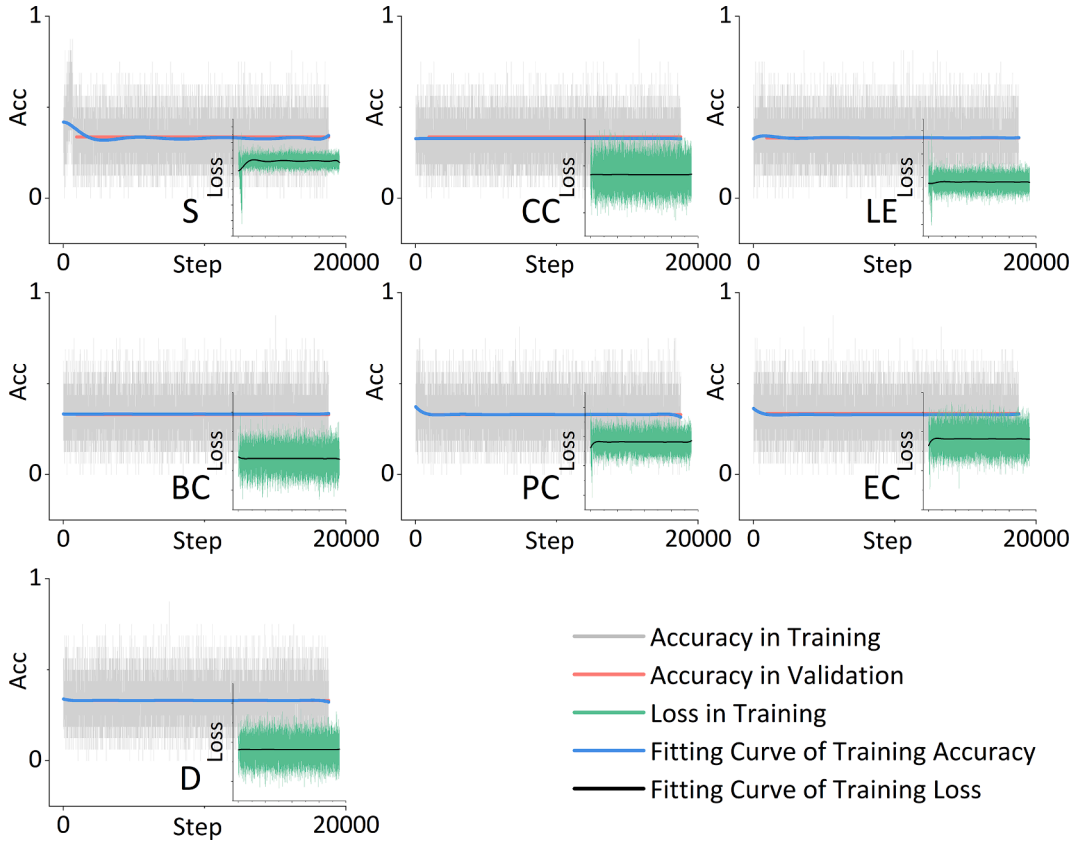


**Fig. 6.** Classification results of regional BCT measures in weighted dynamic brain connectivity without outliers' removal.

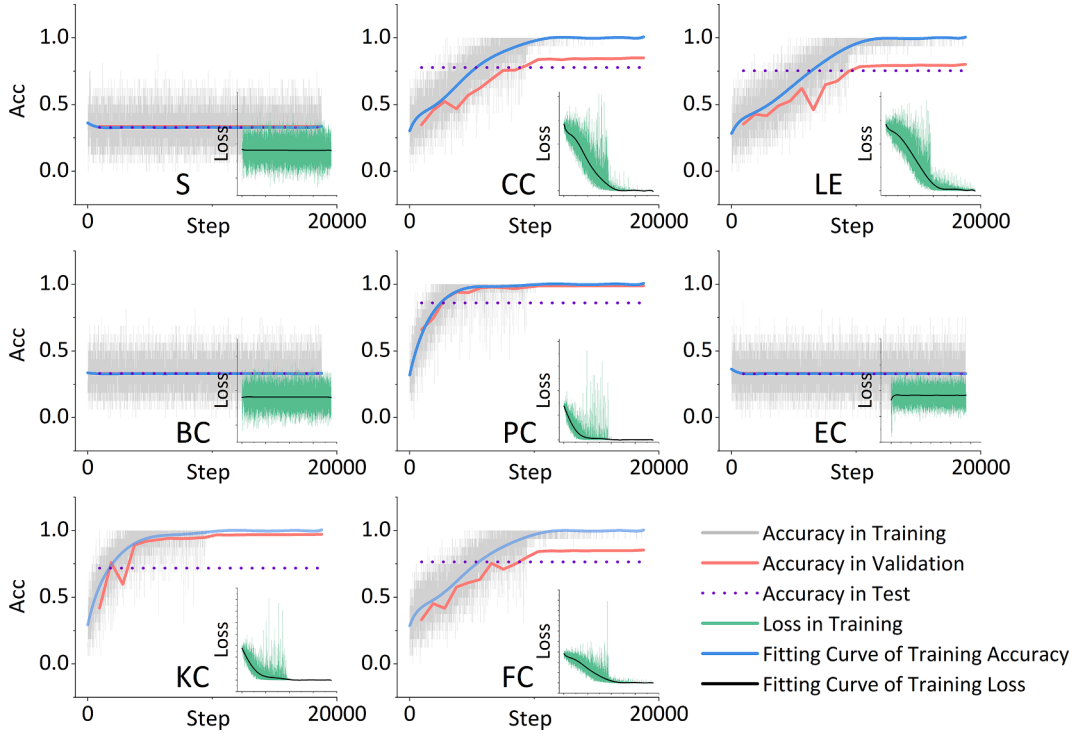


**Fig. 7.** Classification results of regional BCT measures in binary dynamic brain connectivity after statistical outlier removal.

changes in human cognitive ability [25–28], while few studies have a focus on these dedicated multi-modal parcellated cortex regions. In addition to providing more evidence on the primary responsibility of RSN for cognitive impairment of the brain, these fine-grained cortical regions are suggested as the prominent biomarker locations for further studies.

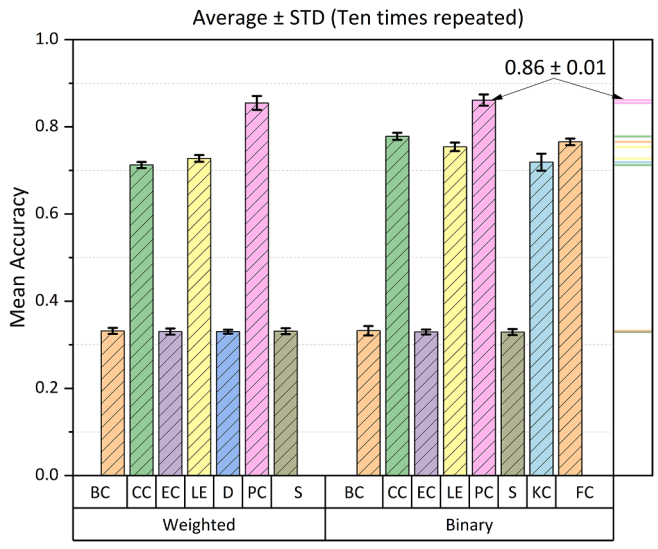


**Fig. 8.** Model test results with error bar in ten times repeated.

### *4.2. Enhanced classification capability in dynamic connectivity with multimodal cortex parcellation and outliers' removal with unsupervised learning*

Although the effectiveness of dynamic connectivity in early cognitive impairment diagnosis has been verified recently, the classification performance is poor, especially in multigroup situations. To date, most studies have achieved high accuracy in binary-group recognition. Ramzan et al., [29] built and validated the ability of a convolutional neural network to distinguish the individual diagnosis of cognitive impairment who will convert to AD with stable MCI with an accuracy of 75%. Li et al., [30] constructed a hypernetwork by integrating ASL perfusion MRI with BOLD fMRI time series and achieved an accuracy of 86.9% for classification in 28 MCI individuals and 33 healthy controls. Ieracitano et al., [31] developed a multimodal feature extraction method based on EEG recordings and obtained an average accuracy of 94.5% with machine learning for any two pairs among HC, MCI, and AD subjects. Table 6 lists the classification performance compared with previous studies. Although it is expected to be the most fine-grained multi-modal cortex parcellation, HCP MMP hasn't been widely studied due to its rigorous requirements for MRI data. Only static connectivity was considered before [11–13]. It can also be observed that for multi-group classification, a high-level accuracy of prediction is difficult. On the one hand, it is limited by the available samples for model learning, especially because the number of MCI or AD patients is far fewer than that of healthy individuals, which leads to a severe imbalance of training data. On the other hand, the single modal based parcellation model or fMRI with static connectivity is inadequate to learn enough knowledge for accurate recognition. The accuracy of the three-group (HC, MCI, and AD) classification is often approximately 70%~85%, while the four-class (HC, EMCI, LMCI, and AD) classification is rarely considered.

In the final test results listed in Table 2, we achieved a superior performance of four-group classification scores of 86.12% with the local BCT measures page rank centrality as input of deep learning. There come two reasons for this. First, dynamic connectivity with a sliding window is constructed, and its effectiveness in the identification of different stages of cognitive impairment is verified. Compared with previous classification results from static connectivity-based studies and the nonparametric significance test, functional connectivity in sliding windowed time series maintains more information about the behavior pattern in the brain. Static connectivity may cause severe loss of subtle functional topological change information in brain regions through homogenization over the scanning period of fMRI time series. It can be observed in the results of Fig. 3 that the difference among groups has increased prominently from static to dynamic. The vast majority of regional BCT measures reached a significance level with a p-value lower than 0.05.

In the box plots of Fig. 4**B**, disadvantages of dynamic connectivity are

**Table 2**
Results for the multigroup classification after deep learning.

| BCT measure | Brain Connectivity | Training | Validation | Test | Previous* |
|---|---|---|---|---|---|
| S | Weighted | 0.3125 | 0.3393 | 0.3311 | 0.7474 |
| PC | Dynamic | 1 | 0.9860 | **0.8548** | – |
| LE | | 1 | 0.7888 | 0.7275 | – |
| EC | | 0.3125 | 0.3303 | 0.3305 | – |
| D | | 0.4375 | 0.3358 | 0.3301 | – |
| CC | | 1 | 0.7968 | 0.7125 | – |
| BC | | 0.4375 | 0.3335 | 0.3319 | – |
| S | Binary | 0.4375 | 0.3368 | 0.3292 | – |
| FC | Dynamic | 1 | 0.8538 | 0.7654 | – |
| PC | | 1 | 0.9883 | **0.8612** | 0.8000 |
| LE | | 1 | 0.8018 | 0.7541 | 0.7684 |
| KC | | 1 | 0.9718 | 0.7188 | 0.7895 |
| EC | | 0.375 | 0.3338 | 0.3294 | 0.7789 |
| CC | | 1 | 0.8498 | 0.7780 | – |
| BC | | 0.1875 | 0.3325 | 0.3324 | 0.7684 |

* Study from [24].

| PC Binary | | Prediction HC | EMCI | LMCI | AD |
|---|---|---|---|---|---|
| True | HC | 872 | 44 | 43 | 46 |
| | EMCI | 68 | 1044 | 67 | 68 |
| | LMCI | 27 | 32 | 703 | 31 |
| | AD | 29 | 33 | 33 | 612 |
| Accuracy = 0.86 | | | | Recall = 0.87 | |
| Precision = 0.86 | | | | F1-score = 0.86 | |

| CC Binary | | Prediction HC | EMCI | LMCI | AD |
|---|---|---|---|---|---|
| True | HC | 793 | 96 | 67 | 57 |
| | EMCI | 97 | 1000 | 74 | 68 |
| | LMCI | 66 | 80 | 603 | 45 |
| | AD | 60 | 69 | 54 | 522 |
| Accuracy = 0.78 | | | | Recall = 0.77 | |
| Precision = 0.77 | | | | F1-score = 0.78 | |

| LE Binary | | Prediction HC | EMCI | LMCI | AD |
|---|---|---|---|---|---|
| True | HC | 754 | 119 | 69 | 61 |
| | EMCI | 98 | 996 | 89 | 72 |
| | LMCI | 70 | 97 | 567 | 56 |
| | AD | 59 | 83 | 50 | 510 |
| Accuracy = 0.75 | | | | Recall = 0.75 | |
| Precision = 0.75 | | | | F1-score = 0.75 | |

| FC Binary | | Prediction HC | EMCI | LMCI | AD |
|---|---|---|---|---|---|
| True | HC | 772 | 107 | 75 | 62 |
| | EMCI | 93 | 1009 | 83 | 65 |
| | LMCI | 59 | 83 | 596 | 46 |
| | AD | 68 | 78 | 62 | 493 |
| Accuracy = 0.77 | | | | Recall = 0.76 | |
| Precision = 0.76 | | | | F1-score = 0.76 | |

**Fig.9.** Confusion Matrix corresponding to the tested model.

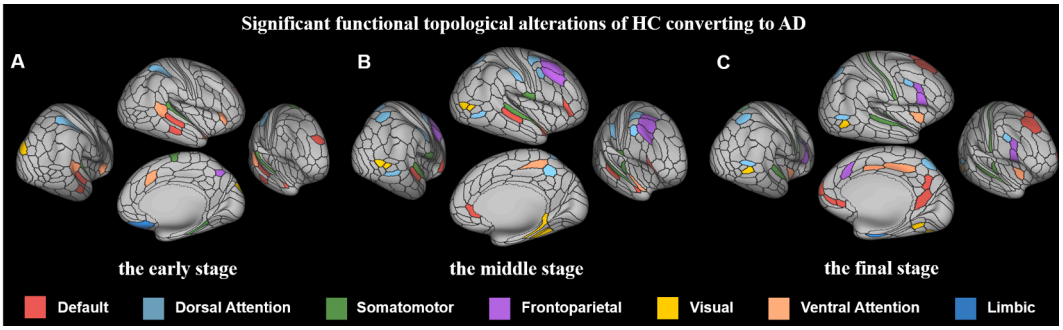


**Fig. 10.** Significant ($p < 0.05$) functional topological alterations from HCs converting to AD.

**Table 3**
Cortical Areas referred in Fig. 10A.

| Stage | Area Name in HCP MMP | Area Description [10] | Corresponds to RSN |
|---|---|---|---|
| The early stage (HCs to EMCI) | R-9p | Area 9 Posterior | DMN |
| | R-STSdp | Area STSd posterior | |
| | L-STGa | Area STGa | |
| | L-TE1m | Area TE1 Middle | |
| | R-p32pr | Area p32 prime | VAN |
| | R-TPOJ1 | Area TemporoParietoOccipital Junction 1 | |
| | L-FOP5 | Area Frontal Opercular 5 | |
| | R-A4 | Auditory 4 Complex | SN |
| | L-6mp | Area 6mp | |
| | R-V3A | Area V3A | VN |
| | L-PHA1 | ParaHippocampal Area 1 | |
| | L-AIP | Anterior IntraParietal Area | DAN |
| | L-7Pm | Medial Area 7P | FN |
| | L-OFC | Orbital Frontal Complex | Limbic system |

**Table 4**
Cortical Areas referred in Fig. 10B.

| Stage | Area Name in HCP MMP | Area Description [10] | Corresponds to RSN |
|---|---|---|---|
| The middle stage (EMCI to LMCI) | R-FEF | Frontal Eye Fields | DAN |
| | R-7AL | Lateral Area 7A | |
| | R-PFt | Area PFt | |
| | R-FST | Area FST | |
| | L-PEF | Premotor Eye Field | |
| | L-LIPV | Area Lateral IntraParietal ventral | |
| | R-STGa | Area STGa | DMN |
| | L-PCV | PreCuneus Visual Area | |
| | L-a24 | Area a24 | |
| | L-45 | Area 45 | |
| | L-STSdp | Area STSd posterior | |
| | R-Pres | PreSubiculum | VN |
| | R-LO3 | Area Lateral Occipital 3 | |
| | L-MT | Middle Temporal Area | |
| | L-Pres | PreSubiculum | |
| | L-PHA3 | ParaHippocampal Area 3 | |
| | L-PHA2 | ParaHippocampal Area 2 | |
| | R-8Av | Area 8Av | FN |
| | L-8c | Area 8c | |
| | L-i6-8 | Inferior 6–8 Transitional Area | |
| | L-OP4 | Area OP4/PV | SN |
| | L-A5 | Auditory 5 Complex | |
| | L-MBelt | Medial Belt Complex | |
| | R-5mv | Area 5 m ventral | VAN |
| | L-PI | Para-Insular Area | |

**Table 5**
Cortical Areas referred in Fig. 10C.

| Stage | Area Name in HCP MMP | Area Description [10] | Corresponds to RSN |
|---|---|---|---|
| The final stage (LMCI to AD) | R-7 *m* | Area 7 *m* | DMN |
| | R-POS1 | Parieto-Occipital Sulcus Area 1 | |
| | R-8Ad | Area 8Ad | |
| | L-10r | Area 10r | |
| | L-10d | Area 10d | |
| | L-s6-8 | Superior 6–8 Transitional Area | |
| | L-s32 | Area s32 | |
| | R-7Am | Medial Area 7A | DAN |
| | R-LIPv | Area Lateral IntraParietal ventral | |
| | R-IFJp | Area IFJp | |
| | R-TPOJ3 | Area TemporoParietoOccipital Junction 3 | |
| | L-7Pl | Lateral Area 7P | |
| | R-23c | Area 23c | VAN |
| | R-p24pr | Area Posterior 24 prime | |
| | R-MI | Middle Insular Area | |
| | R-3a | Area 3a | SN |
| | R-A5 | Auditory 5 Complex | |
| | R-MBelt | Medial Belt Complex | |
| | R-44 | Area 44 | FN |
| | R-IFJa | Area IFJa | |
| | L-a32pr | Area anterior 32 prime | |
| | R-MST | Medial Superior Temporal Area | VN |
| | R-VMV2 | VentroMedial Visual Area 2 | |
| | L-V8 | Eighth Visual Area | |
| | R-EC | Entorhinal Cortex | Limbic system |

prominent, in which too much noise is generated through windowed fMRI time series. The original continuous signal is manually split into multiple overlapping fragments. This causes the regional topological measures to be incorrectly calculated based on these connectivity matrices. The outliers must be removed as the postprocessing step after graph-based complex brain network analysis.

BCT measures are not processed into normal distribution on purpose. First, the natural distribution of BCT measures is unknown. For this reason, we tested the significance with the nonparametric statistical analysis instead of the commonly used *t*-test or ANOVA analysis. We found BCT measures in dynamic connectivity presented more significantly although many outliers were observed in the boxplot. Second, to remove these noisy values, K-means was carried out to differentiate the noise and the valid values (that is why $K = 2$) by unsupervised clustering. After outliers' removal, we found the centralized distributed BCT measures in Fig. 4**A** are approximately normally distributed as shown in Fig. 4**C**.

We compare the classification ability in the static and dynamic connectivity with both weighted and binary networks from Fig. 5 to Fig. 7. In Fig. 5, the training curves of nearly all the regional BCT measures except BC reach a relatively stable high accuracy. Models seem to be good enough for multigroup recognition. In testing, the results fluctuate in the range of 20% ~ 50% only. The models learned are underfitting due to their insufficient training data and inappropriate feature extraction. The results in Fig. 6 and Fig. 7 again demonstrate the

**Table 6**
Classification performance compared with previous studies.

| Method | Number | Modality | Parcellation | Connectivity | Classification | Accuracy |
|---|---|---|---|---|---|---|
| F De Vos et al., (2018) [32] | 250 | fMRI | ICA/RSN | Static/Dynamic | Binary | 79% |
| Anwar et al., (2018) [33] | 287 | sMRI | SPM | – | Three-group | 79.8% |
| Amoroso et al., (2018) [34] | 240 | sMRI | Freesurfer | – | Four-group | 38.8% |
| Sheng et al., (2019) [11] | 96 | sMRI/fMRI | HCP MMP | Static | Binary | 95.8% |
| Huang et al., (2020) [35] | 120 | FA/MD/sMRI | Colin27 | – | Binary | 94.2% |
| Liu et al., (2021) [36] | 560 | sMRI | Freesurfer | – | Binary | 73.8% |
| Basheera et al., (2021) [37] | 349 | sMRI | ICA | – | Three-group | 81.48% |
| Gao et al., (2021) [38] | 1139 | sMRI | FMRIB | – | Three-group | 62.9% |
| Sheng et al., (2021) [12] | 132 | sMRI/fMRI | HCP MMP | Static | Four-group | 53.3% |
| **Proposed** | 160 | sMRI/fMRI | HCP MMP | Dynamic | Four-group | 86% |

better performance of the DBCP method than the original regional BCT measures in dynamic connectivity without processing abnormal values. There are almost no changes in the curves of Fig. 6, which depicts the ineffectiveness of dynamic connectivity before post-processing in DBCP. Too many outliers (see Fig. 4**B**) along with thousands of training steps result in no useful weightings being searched during the training procedure. Most measures shown in Fig. 7 achieve high classification scores in both training and testing. The pagerank centrality measures the importance of nodes in a graph, assigns scores to these nodes, and performs ranking on them. It was initially proposed for a proper ranking of web pages [39], and recently, it has been applied successfully in the domain of MCI or AD prediction [40–42]. Ebadi et al., [43] collected 45 adults for training in various machine learning algorithms and identified the page rank measure in the premotor cortex as one of the good discriminative features for MCI diagnosis. Khazaee et al., calculated 5 global and 2,904 local BCT measures in 168 subjects of the ADNI dataset and found that the local page rank was able to classify three groups with an accuracy of 80%. Moreover, it was confirmed as the optimal functional topological feature in brain connectivity for the recognition of HC, MCI, and AD [24]. For the clustering coefficient measure, de Vos et al., [32] investigated 77 AD patients and 173 controls using RS-fMRI data, calculated graph-based connectivity measures, and finally achieved an AUC (area under the receiver operating characteristic curve) score of 0.84. Josefsson et al., [44] verified the significant difference of clustering coefficient measure of EEG recordings between the subject of MCI and healthy controls. The results in this study agree with previous studies that page rank and clustering coefficient are suitable for the usage of recognition in MCI and AD groups and improve the accuracy substantially to 86.12% in four-group classification by the DBCP method.

### *4.3. Effective deep learning structure in DBCP for multigroup classification*

In addition to the outstanding performance in statistical significance tests, dynamic connectivity solves the problem of few available samples in static functional connectivity analysis. Due to the small proportion of cognitive impairment patients in the population and various inconsistent imaging protocols, valid data for training are insufficient compared with other deep learning studies. In this study, we collected 160 subjects from four groups as much as possible to construct static connectivity. For dynamic connectivity, the number of available samples is enlarged to 20,000 as a result of the sliding window. Each segmented connectivity within windowed time series is regarded as an instance of brain behavior patterns among EMCI, LMCI, AD, or HC. Another feature of deep learning in this study is that the acquired dataset is divided into three parts. During the learning procedure, only the training and validation sets are used in the epoch iterations. Weights in the model are regulated toward a better performance with validation data. As mentioned in previous studies, two-part holdout strategy would induce overfitting in classification. Therefore, the test set is used only once to test the true ability of the learned model in multigroup recognition. Other parameters are tested through replication experiments. As illustrated in Fig. 11, the learning rate of 0.0001 is determined by its highest accuracy.

Various deep learning models are being designed in studies. Except for the recognition performance in different groups, too complex a model structure and such many parameters to be adjusted dramatically increase the difficulty of training. Commonly used structures, including CNNs, RNNs, or other models, always involve hundreds of layers, nodes, and customized settings, which reduce the reproducibility of the results. The poor interpretability of complex deep learning models is also one of the commonly confused problems in the early prediction of MCI. Regardless of how complexly the learning model is designed, it is essentially a fully connected neural network structure. In this study, with the help of the DBCP method, the outstanding performance of multigroup recognition is built on a simple and standard deep learning module with a four-hidden layer and a softmax function. It is entirely dependent on the superiority of dynamic connectivity mapping with HCP MMP and interference information removal in the postprocessing stage.

Several aspects can be improved in future study. First, the construction of connectivity can be more specific to explore the cooperative mechanism in the brain. Correlation coefficient between fMRI signals is the most efficient and widely used approach to evaluate the linear coupling degree in brain areas, while intrinsic information may be hidden by this simple mathematical calculation. Physiological characteristics like phase synchronization [45] and time delay stability [46] can be exploited to assess the complex brain systems, especially for dynamic connectivity construction and pathological brain analysis [47,48]. Second, although we have tried our best to reduce the impact of overfitting, the only way to avoid overfitting is to expand the available samples as much as possible. The small size of AD samples is still a common problem that hinders the application of deep learning in AD study.

## 5. Conclusion

Following a series of processing steps in DBCP and mapping with HCP MMP, centrality alterations in the DMN and DAN show predominant responsibility for cognitive impairment in the brain. Multigroup classification capability is enhanced with statistical outliers recognized in the K-means algorithm. Dynamic functional connectivity within the most fine-grained multimodal human cortex parcellation is demonstrated with prominent performance in analysis and recognition for different stages of HC conversion to AD. The DBCP preprocessing platform is available (https://dbcp.cuz.edu.cn and https://github.com/Bocheng-Wang/DBCP), which allows great freedom in usage.

## Data availability statement

All data are available on request. The DBCP preprocessing platform is available (http://dbcp.cuz.edu.cn and https://github.com/Bocheng-Wang/DBCP), which allows great freedom in usage.

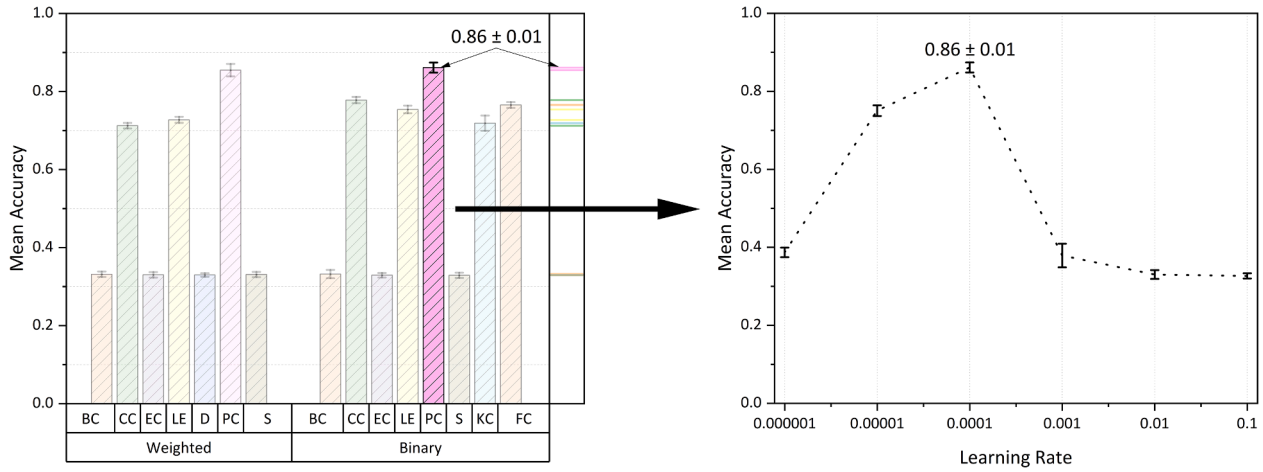


**Fig. 11.** Classification performance with different learning rates.

*CRediT authorship contribution statement*

**Bocheng Wang:** Conceptualization, Methodology, Software, Visualization. **Lei Li:** Investigation, Data curation, Validation. **Long Peng:** Investigation, Data curation, Validation. **Zhuolin Jiang:** Investigation, Data curation. **Kexuan Dai:** Investigation, Data curation. **Qi Xie:** Investigation. **Yue Cao:** Investigation. **Dingguo Yu:** Resources.

## Declaration of Competing Interest

The authors declare that they have no known competing financial interests or personal relationships that could have appeared to influence the work reported in this paper.

## Acknowledgments

This work was supported by the High-level Scientific Innovation Cultivation Project for Young Doctors in the Communication University of Zhejiang (No.8, 2021). Data collection and sharing for this project was funded by the Alzheimer's Disease Neuroimaging Initiative (ADNI) National Institutes of Health Grant U01 AG024904.

## Appendix A. Supplementary data

Supplementary data to this article can be found online at https://doi.org/10.1016/j.bspc.2022.103725.

## References

[1] S. Sarraf, D.D. DeSouza, J. Anderson, G. Tofighi, for the Alzheimer's disease neuroimaging initiativ, DeepAD: Alzheimer's disease classification via deep convolutional neural networks using MRI and fMRI, Bioinformatics (2016), https://doi.org/10.1101/070441.

[2] K. Hu, Y. Wang, K. Chen, L. Hou, X. Zhang, Multi-scale features extraction from baseline structure MRI for MCI patient classification and AD early diagnosis, Neurocomputing. 175 (2016) 132–145, https://doi.org/10.1016/j.neucom.2015.10.043.

[3] S.H. Hojjati, A. Ebrahimzadeh, A. Khazaee, A. Babajani-Feremi, A.D.N. Initiative, others, Predicting conversion from MCI to AD using resting-state fMRI, graph theoretical approach and SVM, J. Neurosci. Methods 282 (2017) 69–80.

[4] M. Pagani, F. Nobili, S. Morbelli, D. Arnaldi, A. Giuliani, J. Öberg, N. Girtler, A. Brugnolo, A. Picco, M. Bauckneht, R. Piva, A. Chincarini, G. Sambuceti, C. Jonsson, F. De Carli, Early identification of MCI converting to AD: a FDG PET study, Eur J Nucl Med Mol Imaging. 44 (2017) 2042–2052, https://doi.org/10.1007/s00259-017-3761-x.

[5] S. Tsartsalis, A. Xekardaki, P.R. Hof, E. Kövari, C. Bouras, Early Alzheimer-type lesions in cognitively normal subjects, Neurobiol. Aging 62 (2018) 34–44, https://doi.org/10.1016/j.neurobiolaging.2017.10.002.

[6] J. Liu, J. Wang, B. Hu, F.-X. Wu, Y. Pan, Alzheimer's Disease Classification Based on Individual Hierarchical Networks Constructed With 3-D Texture Features, IEEE Trans.on Nanobioscience. 16 (2017) 428–437, https://doi.org/10.1109/TNB.2017.2707139.

[7] S.H. Hojjati, A. Ebrahimzadeh, A. Khazaee, A. Babajani-Feremi, Predicting conversion from MCI to AD by integrating rs-fMRI and structural MRI, Comput. Biol. Med. 102 (2018) 30–39, https://doi.org/10.1016/j.compbiomed.2018.09.004.

[8] H.-I. Suk, S.-W. Lee, D. Shen, Latent feature representation with stacked auto-encoder for AD/MCI diagnosis, Brain Struct Funct 220 (2) (2015) 841–859.

[9] K.A. Grajski, S.L. Bressler, Differential medial temporal lobe and default-mode network functional connectivity and morphometric changes in Alzheimer's disease, NeuroImage: Clinical. 23 (2019), 101860, https://doi.org/10.1016/j.nicl.2019.101860.

[10] M.F. Glasser, T.S. Coalson, E.C. Robinson, C.D. Hacker, J. Harwell, E. Yacoub, K. Ugurbil, J. Andersson, C.F. Beckmann, M. Jenkinson, S.M. Smith, D.C. Van Essen, A multi-modal parcellation of human cerebral cortex, Nature 536 (7615) (2016) 171–178.

[11] J. Sheng, B. Wang, Q. Zhang, Q. Liu, Y. Ma, W. Liu, M. Shao, B. Chen, A novel joint HCPMMP method for automatically classifying Alzheimer's and different stage MCI patients, Behav. Brain Res. 365 (2019) 210–221, https://doi.org/10.1016/j.bbr.2019.03.004.

[12] J. Sheng, B. Wang, Q. Zhang, R. Zhou, L. Wang, Y. Xin, Identifying and characterizing different stages toward Alzheimer's disease using ordered core features and machine learning, Heliyon. 7 (2021) e07287. https://doi.org/10.1016/j.heliyon.2021.e07287.

[13] J. Sheng, B. Wang, Q. Zhang, M. Yu, Connectivity and variability of related cognitive subregions lead to different stages of progression toward Alzheimer's disease, Heliyon. (2022) e08827.

[14] U. Pervaiz, D. Vidaurre, M.W. Woolrich, S.M. Smith, Optimising network modelling methods for fMRI, NeuroImage. 211 (2020), 116604.

[15] V.D. Calhoun, R. Miller, G. Pearlson, T. Adalı, The chronnectome: time-varying connectivity networks as the next frontier in fMRI data discovery, Neuron 84 (2014) 262–274.

[16] P. Toiviainen, I. Burunat, E. Brattico, P. Vuust, V. Alluri, The chronnectome of musical beat, NeuroImage. 216 (2020), 116191, https://doi.org/10.1016/j.neuroimage.2019.116191.

[17] J. Liu, X. Liao, M. Xia, Y. He, Chronnectome fingerprinting: Identifying individuals and predicting higher cognitive functions using dynamic brain connectivity patterns, Hum. Brain Mapp. 39 (2018) 902–915, https://doi.org/10.1002/hbm.23890.

[18] E. Premi, V.D. Calhoun, M. Diano, S. Gazzina, M. Cosseddu, A. Alberici, S. Archetti, D. Paternicò, R. Gasparotti, J. van Swieten, D. Galimberti, R. Sanchez-Valle, R. Laforce, F. Moreno, M. Synofzik, C. Graff, M. Masellis, M.C. Tartaglia, J. Rowe, R. Vandenberghe, E. Finger, F. Tagliavini, A. de Mendonça, I. Santana, C. Butler, S. Ducharme, A. Gerhard, A. Danek, J. Levin, M. Otto, G. Frisoni, S. Cappa, S. Sorbi, A. Padovani, J.D. Rohrer, B. Borroni, M.R. Almeida, S. Anderl-Straub, C. Andersson, A. Antonell, A. Arighi, M. Balasa, M. Barandiaran, N. Bargalló, R. Bartha, B. Bender, L. Benussi, G. Binetti, S. Black, M. Bocchetta, S. Borrego-Ecija, J. Bras, R. Bruffaerts, P. Caroppo, D. Cash, M. Castelo-Branco, R. Convery, T. Cope, M. de Arriba, G. Di Fede, Z. Díaz, K.M. Dick, D. Duro, C. Fenoglio, C. Ferreira, C. B. Ferreira, T. Flanagan, N. Fox, M. Freedman, G. Fumagalli, A. Gabilondo, S. Gauthier, R. Ghidoni, G. Giaccone, A. Gorostidi, C. Greaves, R. Guerreiro, C. Heller, T. Hoegen, B. Indakoetxea, V. Jelic, L. Jiskoot, H.-O. Karnath, R. Keren, M.J. Leitão, A. Lladó, G. Lombardi, S. Loosli, C. Maruta, S. Mead, L. Meeter, G. Miltenberger, R. van Minkelen, S. Mitchell, B. Nacmias, M. Neason, J. Nicholas, L. Öijerstedt, J. Olives, J. Panman, J. Papma, M. Patzig, M. Pievani, S. Prioni, C. Prix, R. Rademakers, V. Redaelli, T. Rittman, E. Rogaeva, P. Rosa-Neto, G. Rossi, M. Rossor, B. Santiago, E. Scarpini, E. Semler, R. Shafei, C. Shoesmith, M. Tábuas-Pereira, M. Tainta, D. Tang-Wai, D.L. Thomas, H. Thonberg, C. Timberlake, P. Tiraboschi, P. Vandamme, M. Vandenbulcke, M. Veldsman, A. Verdelho, J. Villanua, J. Warren, C. Wilke, H. Zetterberg, M. Zulaica, The inner fluctuations

of the brain in presymptomatic Frontotemporal Dementia: The chronnectome fingerprint, NeuroImage. 189 (2019) 645–654, https://doi.org/10.1016/j.neuroimage.2019.01.080.
[19] S. Moguilner, A.M. García, Y.S. Perl, E. Tagliazucchi, O. Piguet, F. Kumfor, P. Reyes, D. Matallana, L. Sedeño, A. Ibáñez, Dynamic brain fluctuations outperform connectivity measures and mirror pathophysiological profiles across dementia subtypes: A multicenter study, NeuroImage. 225 (2021), 117522, https://doi.org/10.1016/j.neuroimage.2020.117522.
[20] B.T. Thomas Yeo, F.M. Krienen, J. Sepulcre, M.R. Sabuncu, D. Lashkari, M. Hollinshead, J.L. Roffman, J.W. Smoller, L. Zöllei, J.R. Polimeni, B. Fischl, H. Liu, R.L. Buckner, The organization of the human cerebral cortex estimated by intrinsic functional connectivity, J. Neurophysiol. 106 (3) (2011) 1125–1165.
[21] M.F. Glasser, S.N. Sotiropoulos, J.A. Wilson, T.S. Coalson, B. Fischl, J.L. Andersson, J. Xu, S. Jbabdi, M. Webster, J.R. Polimeni, D.C. Van Essen, M. Jenkinson, The minimal preprocessing pipelines for the Human Connectome Project, Neuroimage. 80 (2013) 105–124.
[22] M. Rubinov, O. Sporns, Complex network measures of brain connectivity: Uses and interpretations, NeuroImage. 52 (2010) 1059–1069, https://doi.org/10.1016/j.neuroimage.2009.10.003.
[23] H.u. Cheng, Y. Wang, J. Sheng, W.G. Kronenberger, V.P. Mathews, T.A. Hummer, A.J. Saykin, Characteristics and variability of structural networks derived from diffusion tensor imaging, Neuroimage. 61 (4) (2012) 1153–1164.
[24] A. Khazaee, A. Ebrahimzadeh, A. Babajani-Feremi, Application of advanced machine learning methods on resting-state fMRI network for identification of mild cognitive impairment and Alzheimer's disease, Brain Imaging and Behavior. 10 (2016) 799–817, https://doi.org/10.1007/s11682-015-9448-7.
[25] N. Franzmeier, K. Buerger, S. Teipel, Y. Stern, M. Dichgans, M. Ewers, Cognitive reserve moderates the association between functional network anti-correlations and memory in MCI, Neurobiol. Aging 50 (2017) 152–162, https://doi.org/10.1016/j.neurobiolaging.2016.11.013.
[26] Z. Wang, V.J. Williams, K.A. Stephens, C. Kim, L. Bai, M. Zhang, D.H. Salat, The effect of white matter signal abnormalities on default mode network connectivity in mild cognitive impairment, Hum Brain Mapp. 41 (2020) 1237–1248, https://doi.org/10.1002/hbm.24871.
[27] F. Miraglia, F. Vecchio, C. Marra, D. Quaranta, F. Alù, B. Peroni, G. Granata, E. Judica, M. Cotelli, P.M. Rossini, Small World Index in Default Mode Network Predicts Progression from Mild Cognitive Impairment to Dementia, Int. J. Neur. Syst. 30 (2020) 2050004, https://doi.org/10.1142/S0129065720500045.
[28] L.T. Eyler, J.A. Elman, S.N. Hatton, S. Gough, A.K. Mischel, D.J. Hagler, C.E. Franz, A. Docherty, C. Fennema-Notestine, N. Gillespie, D. Gustavson, M.J. Lyons, M. C. Neale, M.S. Panizzon, A.M. Dale, W.S. Kremen, R. Perneczky, Resting State Abnormalities of the Default Mode Network in Mild Cognitive Impairment: A Systematic Review and Meta-Analysis, JAD. 70 (1) (2019) 107–120.
[29] F. Ramzan, M.U.G. Khan, A. Rehmat, S. Iqbal, T. Saba, A. Rehman, Z. Mehmood, A Deep Learning Approach for Automated Diagnosis and Multi-Class Classification of Alzheimer's Disease Stages Using Resting-State fMRI and Residual Neural Networks, J Med Syst. 44 (2020) 37, https://doi.org/10.1007/s10916-019-1475-2.
[30] Y. Li, J. Liu, X. Gao, B. Jie, M. Kim, P.-T. Yap, C.-Y. Wee, D. Shen, Multimodal hyper-connectivity of functional networks using functionally-weighted LASSO for MCI classification, Med. Image Anal. 52 (2019) 80–96, https://doi.org/10.1016/j.media.2018.11.006.
[31] C. Ieracitano, N. Mammone, A. Hussain, F.C. Morabito, A novel multi-modal machine learning based approach for automatic classification of EEG recordings in dementia, Neural Networks. 123 (2020) 176–190, https://doi.org/10.1016/j.neunet.2019.12.006.
[32] F. de Vos, M. Koini, T.M. Schouten, S. Seiler, J. van der Grond, A. Lechner, R. Schmidt, M. de Rooij, S.A.R.B. Rombouts, A comprehensive analysis of resting state fMRI measures to classify individual patients with Alzheimer's disease, NeuroImage. 167 (2018) 62–72, https://doi.org/10.1016/j.neuroimage.2017.11.025.
[33] T. Altaf, S.M. Anwar, N. Gul, M.N. Majeed, M. Majid, Multi-class Alzheimer's disease classification using image and clinical features, Biomed. Signal Process. Control 43 (2018) 64–74, https://doi.org/10.1016/j.bspc.2018.02.019.
[34] N. Amoroso, D. Diacono, A. Fanizzi, M. La Rocca, A. Monaco, A. Lombardi, C. Guaragnella, R. Bellotti, S. Tangaro, Deep learning reveals Alzheimer's disease onset in MCI subjects: Results from an international challenge, J. Neurosci. Methods 302 (2018) 3–9, https://doi.org/10.1016/j.jneumeth.2017.12.011.
[35] L. Kang, J. Jiang, J. Huang, T. Zhang, Identifying Early Mild Cognitive Impairment by Multi-Modality MRI-Based Deep Learning, Front. Aging Neurosci. 12 (2020) 206, https://doi.org/10.3389/fnagi.2020.00206.
[36] X. Tang, J. Liu, Comparing different algorithms for the course of Alzheimer's disease using machine learning, Ann Palliat Med. 10 (2021) 9715–9724. https://doi.org/10.21037/apm-21-2013.
[37] S. Basheera, M.S.S. Ram, Deep learning based Alzheimer's disease early diagnosis using T2w segmented gray matter MRI, Int J Imaging Syst Technol. 31 (2021) 1692–1710, https://doi.org/10.1002/ima.22553.
[38] Z. Zhang, L. Gao, G. Jin, L. Guo, Y. Yao, L.i. Dong, J. Han, THAN: task-driven hierarchical attention network for the diagnosis of mild cognitive impairment and Alzheimer's disease, Quant Imaging Med Surg 11 (7) (2021) 3338–3354.
[39] A. Hashemi, M.B. Dowlatshahi, H. Nezamabadi-pour, MGFS: A multi-label graph-based feature selection algorithm via PageRank centrality, Expert Syst. Appl. 142 (2020), 113024, https://doi.org/10.1016/j.eswa.2019.113024.
[40] J. Neudorf, C. Ekstrand, S. Kress, R. Borowsky, Brain Structural Connectivity Predicts Brain Functional Complexity: Diffusion Tensor Imaging Derived Centrality Accounts for Variance in Fractal Properties of Functional Magnetic Resonance Imaging Signal, Neuroscience 438 (2020) 1–8, https://doi.org/10.1016/j.neuroscience.2020.04.048.
[41] J. Kelly, R. Moyeed, C. Carroll, S. Luo, X. Li, Genetic networks in Parkinson's and Alzheimer's disease, Aging. 12 (2020) 5221–5243. https://doi.org/10.18632/aging.102943.
[42] L.R. Peraza, A. Díaz-Parra, O. Kennion, D. Moratal, J.-P. Taylor, M. Kaiser, R. Bauer, Alzheimer's Disease Neuroimaging Initiative, Structural connectivity centrality changes mark the path toward Alzheimer's disease, Alzheimer's & Dementia: Diagnosis, Assessment & Disease Monitoring. 11 (1) (2019) 98–107.
[43] D. Yao, V.D. Calhoun, Z. Fu, Y. Du, J. Sui, An ensemble learning system for a 4-way classification of Alzheimer's disease and mild cognitive impairment, J. Neurosci. Methods 302 (2018) 75–81, https://doi.org/10.1016/j.jneumeth.2018.03.008.
[44] A. Josefsson, A. Ibáñez, M. Parra, J. Escudero, Network analysis through the use of joint-distribution entropy on EEG recordings of MCI patients during a visual short-term memory binding task, Healthcare Technol. Lett. 6 (2019) 27–31, https://doi.org/10.1049/htl.2018.5060.
[45] R.P. Bartsch, A.Y. Schumann, J.W. Kantelhardt, T. Penzel, P.C. Ivanov, Phase transitions in physiologic coupling, Proc. Natl. Acad. Sci. 109 (26) (2012) 10181–10186.
[46] A. Bashan, R.P. Bartsch, J. Kantelhardt, S. Havlin, P.C. Ivanov, others, Network physiology reveals relations between network topology and physiological function, Nature, Communications. 3 (2012) 1–9.
[47] A. Lin, K.K. Liu, R.P. Bartsch, P.C. Ivanov, Dynamic network interactions among distinct brain rhythms as a hallmark of physiologic state and function, Communications Biology. 3 (2020) 1–11.
[48] E.E. Asher, M. Plotnik, M. Günther, S. Moshel, O. Levy, S. Havlin, J.W. Kantelhardt, R.P. Bartsch, Connectivity of EEG synchronization networks increases for Parkinson's disease patients with freezing of gait, Communications Biology. 4 (2021) 1–10.